RESEARCH ARTICLE

Comparative Simulation of Existing and Proposed Flood Protection Infrastructure Under 10-Year, 25-Year, 50-Year, 100-Year, and 500-Year Design Flood Events Using HEC-RAS 2D.

Dhanush Raghupathy
Cascade Civil Services LLC
Email: dhanushunionly@gmail.com

Received	Revised	Accepted	Published
16 May 2024	22 June 2024	8 August 2024	15 September 2024

Abstract

Background: **Flood**-protection design is often evaluated at a single recurrence interval, leaving uncertainty about residual performance during rarer events.

Objective: This study compares existing protection, a 0.60-m levee increase, detention with 17% event-peak attenuation, and their combination under 10-, 25-, 50-, 100- and 500-year flood scenarios.

Methods: A controlled HEC-RAS 2D hydraulic scenario framework contains 16 cross-sections, 120 floodplain cells and 20 infrastructure–event combinations. Outcomes include flooded area, wet-cell depth, overtopped sections and asset-associated exposure.

Results: Existing protection inundates 37–53 ha; the combined design inundates 31–48 ha, a matched-event reduction of 9.4–16.2%. Mean wet-cell depth decreases by 21.8–23.1%. In the 100-year event, overtopped sections decrease from 16 to one, whereas 15 of 16 remain overtopped at 500 years. Flooded built-up cells decline from 32 to 28 at 100 years and from 35 to 32 at 500 years.

Conclusion: The combined configuration is consistently preferable on the modelled hydraulic indicators, but extreme-event residual exposure remains substantial. The work provides a multi-metric comparison for preliminary infrastructure screening and distinguishes relative protection gains from proof of site-specific design safety.

Keywords: Flood inundation; HEC-RAS 2D; levee design; detention storage; return period; flood risk; hydraulic modelling.

How to cite: Raghupathy D. Comparative Simulation of Existing and Proposed Flood Protection Infrastructure Under 10-Year, 25-Year, 50-Year, 100-Year, and 500-Year Design Flood Events Using HEC-RAS 2D. Int J Bus Comput Sci. 2024.

1. Introduction

Flood defences are commonly designed against a nominal recurrence interval, although infrastructure performance depends on the interaction of peak discharge, flow routing, local conveyance and the spatial distribution of exposed assets. Two-dimensional flood models are useful precisely because sections with comparable water levels can produce different inundation patterns once topographic connectivity, terrain elevation and protection geometry are considered [1]–[4]. Contemporary flood-risk assessments therefore require more than a binary distinction between a protected and an unprotected floodplain [5]–[8].

The representation of rare events remains particularly consequential. Regional and global inundation studies demonstrate that return-period mapping can materially alter estimates of people and infrastructure exposed to flooding [9]–[12]. However, a nominal protection standard does not indicate how a defence fails, where flooding persists or whether a design that controls a moderate event performs proportionately under an extreme event [13]–[15]. Analyses of changing flood risk likewise stress the importance of examining residual exposure rather than assuming that a structural measure can remove it [16]–[21].

Comparative infrastructure studies often report aggregate flooded area without simultaneously examining channel overtopping, wet-cell depth and land-use-specific exposure. That separation can conceal distinct mechanisms of performance: increasing levee height changes the overtopping threshold, whereas detention attenuates the event hydrograph; a combined design could therefore outperform either intervention without eliminating rare-event flooding. Spatial uncertainty and the reliability of hydraulic representations become more important as the expected recurrence interval increases [22]–[27].

This study evaluates four protection configurations under 10-, 25-, 50-, 100- and 500-year design floods using a structured HEC-RAS 2D hydraulic scenario framework. The objectives are to (i) compare inundation extent and depth across the full design spectrum; (ii) quantify overtopping and exposure of built-up and critical-asset cells; (iii) identify whether the combined design provides consistent benefits; and (iv) distinguish flood mitigation from complete protection. The analysis is a controlled, idealised engineering comparison, not a calibrated prediction for a named municipality.

2. Materials and Methods

2.1 Numerical Domain and Scenario Construction

The reach representation contains 16 surveyed-design cross-sections distributed over a 6.0-km chainage, with widths increasing from 24 to 36 m, bankfull depths ranging from 2.42 to 2.78 m, Manning roughness coefficients of 0.035–0.044 and nominal longitudinal slopes of 0.0019–0.0021. A local floodplain assessment window comprises 120 regular 100 m × 100 m raster cells (1.20 km²; 120 ha), with ground elevations from 109.82 to 112.99 m. Forty cells are marked as containing critical assets and 48 as built-up. These flags denote exposed raster locations, not independently enumerated buildings or facilities.

The hydraulic cases are generated by crossing five design storms with four infrastructure arrangements (20 cases). Return-period rainfalls of 83, 117, 144, 174 and 258 mm in 24 h correspond to design-event peak-flow components of 112, 156, 195, 238 and 345 m³/s, respectively. The hydrograph forcing series spans 24 h at 2-h intervals and includes a 12 m³/s background flow; section-level case comparisons use the separately specified event-flow component. This distinction is retained explicitly rather than conflating total hydrograph maxima with the hydraulic design-case

flow entries. Case parameters and geometry are reported in Table 1.

2.2 Infrastructure Alternatives and Hydraulic Representation

Configuration E retains the existing flood-protection geometry. Configuration L raises the levee crest by 0.60 m without changing the inflow boundary. Configuration D represents a detention basin with 0.08 million m³ nominal storage and an imposed 17% reduction in the event peak-flow component. Configuration C combines the 0.60-m crest increase with the same detention-peak adjustment. The resulting effective event peaks are 92.96, 129.48, 161.85, 197.54 and 286.35 m³/s for detention-containing alternatives, compared with 112, 156, 195, 238 and 345 m³/s for E and L.

The analysis uses the numerical hydraulic response fields associated with the HEC-RAS 2D study design: cross-sectional normal depth, velocity, crest exceedance and raster-cell maximum depth and velocity. The governing depth-averaged continuity and momentum description is conventionally expressed as $\partial h/\partial t + \partial(hu)/\partial x + \partial(hv)/\partial y = q$, with friction and bed-gradient contributions in the two momentum directions [1], [2], [5]. The available analytical record contains the parameterised scenario inputs and outputs; it does not contain solver-native geometry, mesh connectivity or computation logs. Consequently, numerical solution settings and mesh-convergence claims are not attributed to these data. The comparison tests relative patterns in the documented scenarios rather than asserting a newly calibrated hydraulic model.

2.3 Evaluation Metrics and Internal Consistency

For each scenario s, flooded area is $A_s = 1\ \text{ha} \times \Sigma_i I(d_{i,s} > 0)$, because each mapped cell is 1 ha. Mean wet-cell depth is $\bar{d}_s = [\Sigma_i d_{i,s} I(d_{i,s} > 0)]/[\Sigma_i I(d_{i,s} > 0)]$. A relative area improvement is $R_{A,s} = 100(A_E - A_s)/A_E$ at the same return period. Overtopping is counted at 16 cross-sections using the recorded overtopping indicator, while built-up and critical exposure are counted by intersecting wet-cell indicators with the corresponding spatial flags. No monetary loss is inferred from these counts.

A cell-level depth–velocity screening index is defined for comparison as $H_i = d_i(v_i + 0.5)$, with depth in metres, velocity in m/s and the offset in m/s; $H_i \geq 1$ is used as an internal high-index class, not as a validated human-instability or damage threshold. Floodplain exposure and index counts were calculated directly from the 2,400 scenario-cell records. Comparison against the 20-case summary confirmed flooded area, mean wet depth and peak depth; selected summary entries for critical-asset exposure differed from their underlying cell flags by one or two cells. Therefore, all exposure counts in Table 2 and Figure 4 are recomputed consistently from the raster-level records. Overtopping counts were independently reconciled against the 320 section records.

2.4 Comparison Strategy

Outputs are presented by return period and intervention rather than combined into one unweighted average. This preserves differences between frequent and rare design events and avoids implying that a 500-year event has the same likelihood as a 10-year event. Given that the 20 scenarios are deterministic design runs rather than independent observations, no sampling-based significance tests or confidence intervals are assigned. Evaluation instead prioritises absolute impacts (hectares, depths and exposed cells), matched-case percentage changes, spatial structure and residual overtopping. Figures 1–3 and Tables 2–3 reproduce these comparisons.

3. Results

3.1 Flooded Extent and Depth

Across the five design events, the existing configuration inundates 37, 41, 44, 48 and 53 ha, equivalent to 30.8–44.2% of the 120-ha window. The combined alternative yields 31, 35, 37, 41 and 48 ha, respectively; its matched-event area reductions are 16.2%, 14.6%, 15.9%, 14.6% and 9.4% (Table 3; Figure 1). Thus, the combined design produces the smallest area in every event, but its percentage benefit contracts substantially for the most extreme forcing.

Levee raising alone gives reductions of 8.1%, 12.2%, 6.8%, 8.3% and 1.9%; detention alone achieves 5.4%, 7.3%, 6.8%, 8.3% and 1.9%. These results show that neither single intervention dominates under all recurrence intervals. Mean wet-cell depth under existing conditions increases from 0.800 to 1.145 m between the 10- and 500-year floods, compared with 0.620 to 0.882 m under the combined design. Its mean-depth reduction is consistently 21.8–23.1% across the scenarios. Peak gridded depths remain appreciable, however: the combined design has maximum depths of 1.420 m at 10 years and 1.982 m at 500 years, versus 1.780 and 2.434 m under existing protection (Table 2).

3.2 Overtopping and Residual Protection Performance

The existing protection has no overtopped sections at the 10-year event, but experiences overtopping at 5, 15, 16 and 16 cross-sections under the 25-, 50-, 100- and 500-year events. Levee raising prevents overtopping at 25 and 50 years, before overtopping reappears at 9 and 16 sections at 100 and 500 years. Detention prevents overtopping at 25 years but retains 7, 15 and 16 overtopped sections at 50, 100 and 500 years. The combined design limits overtopping to zero sections through the 50-year event, one at 100 years and 15 at 500 years (Figure 2).

These counts reveal a pronounced transition rather than uniform protective effectiveness. At 100 years, the combined intervention reduces overtopping from 16 to one section while still inundating 41 ha. At 500 years, it leaves nearly the entire 16-section reach overtopped and 48 ha inundated. The separation between overtopping and floodplain extent indicates that mapped water can persist from conveyance exceedance and spatial storage even when a section-based defence threshold is not exceeded.

3.3 Exposure and Spatial Hazard

Built-up wet-cell counts under existing protection increase from 25 to 35 across the design spectrum; the combined alternative reduces these to 20, 24, 25, 28 and 32 cells (Table 2). In the 100-year event this represents four fewer wet built-up cells, whereas in the 500-year event only three are removed from inundation. Critical-asset-flagged wet cells are unchanged at 15 in the 10-year event, decrease from 17 to 15 at 25 years and from 19 to 17 at 500 years, but show no reduction at 100 years when computed directly from the cell flags. This underscores why improvements in total area cannot be assumed to protect every asset class.

Under the internally defined $H \geq 1$ class, the existing configuration has 18, 21, 26, 29 and 36 wet cells, compared with 9, 14, 15, 19 and 28 under the combined design. These represent class-count reductions of 50.0%, 33.3%, 42.3%, 34.5% and 22.2%, respectively. The 100- and 500-year depth maps (Figure 3) show that attenuation is spatially concentrated, while low-elevation corridors remain exposed in both designs. No cell becomes newly inundated or has greater maximum depth in the combined alternative than in the corresponding existing case within this deterministic scenario set.

4. Discussion

The first substantive result is the nonlinear effect of design rarity on the relative benefit of protection works. A combined levee-and-detention arrangement consistently reduces inundated area, yet its area reduction falls below 10% in the 500-year event. The outcome is consistent with the distinction between design-standard exceedance and residual risk highlighted in flood mapping and protection-standard studies [13]–[15]. In practice, an intervention can improve several operational indicators while leaving a substantial tail of low-probability, high-consequence exposure; evaluating a scheme solely at its nominal return period would miss that feature.

Second, the interventions act on different mechanisms. Levee raising increases the local crest margin without reducing the boundary flow; detention reduces the event peak by 17% but does not directly alter the crest. Their combination reduces both forcing

and the probability of crest exceedance, explaining the larger difference in overtopped sections than in area. For the 100-year flood, reducing overtopping from 16 sections to one is meaningful for pathway control, but the remaining 41-ha inundation footprint indicates that channel capacity, floodplain topography and hydraulic connectivity must be investigated before equivalently large improvements in land protection are claimed. The general need to preserve channel–floodplain exchange is well established in hydraulic-model comparisons [1], [5], [24].

Third, mean depth and area need not change proportionately. The mean wet-cell depth improvement stays near 23% from 10 to 500 years, whereas flooded-area benefits deteriorate as progressively more peripheral cells become wet. This pattern suggests that structural interventions are more effective at attenuating local hydraulic intensity than entirely preventing inundation at the edge of the extreme-event floodplain. Spatial resolution and topographic quality therefore matter when translating these changes into property-level decisions [6]–[8], [25]–[27]. The 100-m raster used here is appropriate for a controlled comparison but cannot resolve kerbs, road embankments, building-scale routes or narrow drainage openings.

Fourth, a reduction in the number of flooded built-up cells does not necessarily imply comparable changes in critical-facility exposure. The 100-year case illustrates this distinction: the combined scenario reduces flooded area by seven hectares but does not reduce wet critical-asset cells when the underlying flags are counted consistently. Similar concerns motivate integrated hazard–exposure frameworks and avoidance of equating wetted area with economic damage [18]–[21]. Future decision appraisal would require asset valuation, vulnerability functions, spatially explicit critical-service dependency and an accepted consequence metric before any benefit–cost ratio or statement on avoided damages could be justified.

Finally, the increasing residual impact under 500-year forcing argues for layered flood-risk management. Structural improvements should be assessed alongside land-use control, emergency access, warning arrangements and consequence-reduction measures, because rare-event failure can remain substantial even under a combined structural configuration [15]–[17], [19], [28]. The present experiment supports prioritising the combined design for further engineering development, not treating its 0.60-m elevation increment or 17% peak attenuation as universally optimal values. Optimisation would require construction cost, available detention volume, routing dynamics, uncertain inflow, freeboard requirements and downstream transfer effects.

5. Conclusion

The comparison of 20 design-flood cases shows that combining a 0.60-m levee increase with a 17% reduction in event peak discharge gives the lowest flooded area and mean depth across all five return periods. Relative to existing protection, the combined alternative reduces flooded area by 14.6% in the 100-year event and 9.4% in the 500-year event; its mean wet-cell depth is reduced by approximately 23%. At the same time, 15 of 16 cross-sections remain overtopped in the 500-year case and 48 ha remain inundated. Structural mitigation therefore improves the distribution of hydraulic hazard without providing an extreme-event guarantee. The findings support a multi-metric appraisal of flood defences that combines area, depth, crest exceedance and location-specific exposure, followed by full hydraulic verification before real-world design adoption.

References

1. M. S. Horritt and P. D. Bates, "Evaluation of 1D and 2D numerical models for predicting river flood inundation," Journal of Hydrology, vol. 268, pp. 87–99, 2002, doi: 10.1016/S0022-1694(02)00121-X.
2. P. D. Bates, M. S. Horritt, and T. J. Fewtrell, "A simple inertial formulation of the shallow water equations for efficient two-dimensional flood inundation modelling," Journal of Hydrology, vol. 387, pp. 33–45, 2010, doi: 10.1016/j.jhydrol.2010.03.027.
3. J. Teng, A. J. Jakeman, J. Vaze, B. F. W. Croke, D. Dutta, and S. Kim, "Flood inundation modelling: A review of methods, recent advances and uncertainty analysis," Environmental Modelling & Software, vol. 90, pp. 201–216, 2017, doi: 10.1016/j.envsoft.2017.01.006.
4. N. M. Hunter, P. D. Bates, M. S. Horritt, and M. D. Wilson, "Simple spatially-distributed models for predicting flood inundation: A review," Geomorphology, vol. 90, pp. 208–225, 2007, doi: 10.1016/j.geomorph.2006.10.021.
5. J. Neal, G. Schumann, and P. Bates, "A subgrid channel model for simulating river hydraulics and floodplain inundation over large and data sparse areas," Water Resources Research, vol. 48, art. W11506, 2012, doi: 10.1029/2012WR012514.
6. A. Alipour, K. Jafarzadegan, and H. Moradkhani, "Global sensitivity analysis in hydrodynamic modeling and flood inundation mapping," Environmental Modelling & Software, vol. 152, art. 105398, 2022, doi: 10.1016/j.envsoft.2022.105398.
7. J. E. Schubert and B. F. Sanders, "Building treatments for urban flood inundation models and implications for predictive skill and modeling efficiency," Advances in Water Resources, vol. 41, pp. 49–64, 2012, doi: 10.1016/j.advwatres.2012.02.012.
8. T. J. Fewtrell, P. D. Bates, M. S. Horritt, and N. M. Hunter, "Evaluating the effect of scale in flood inundation modelling in urban environments," Hydrological Processes, vol. 22, pp. 5107–5118, 2008, doi: 10.1002/hyp.7148.
9. F. Dottori, P. Salamon, A. Bianchi, L. Alfieri, F. A. Hirpa, and L. Feyen, "Development and evaluation of a framework for global flood hazard mapping," Advances in Water Resources, vol. 94, pp. 87–102, 2016, doi: 10.1016/j.advwatres.2016.05.002.
10. C. C. Sampson, A. M. Smith, P. D. Bates, J. C. Neal, L. Alfieri, and J. E. Freer, "A high-resolution global flood hazard model," Water Resources Research, vol. 51, pp. 7358–7381, 2015, doi: 10.1002/2015WR016954.
11. O. E. J. Wing et al., "Estimates of present and future flood risk in the conterminous United States," Environmental Research Letters, vol. 13, art. 034023, 2018, doi: 10.1088/1748-9326/aaac65.
12. O. E. J. Wing et al., "Toward global stochastic river flood modeling," Water Resources Research, vol. 56, art. e2020WR027692, 2020, doi: 10.1029/2020WR027692.
13. H. de Moel, J. van Alphen, and J. C. J. H. Aerts, "Flood maps in Europe—methods, availability and use," Natural Hazards and Earth System Sciences, vol. 9, pp. 289–301, 2009, doi: 10.5194/nhess-9-289-2009.
14. P. Scussolini et al., "FLOPROS: An evolving global database of flood protection standards," Natural Hazards and Earth System Sciences, vol. 16, pp. 1049–1061, 2016, doi: 10.5194/nhess-16-1049-2016.
15. B. Merz, J. Hall, M. Disse, and A. Schumann, "Fluvial flood risk management in a changing world," Natural Hazards and Earth System Sciences, vol. 10, pp. 509–527, 2010, doi: 10.5194/nhess-10-509-2010.
16. F. Dottori et al., "Increased human and economic losses from river flooding with anthropogenic warming," Nature Climate Change, vol. 8, pp. 781–786, 2018, doi: 10.1038/s41558-018-0257-z.
17. H. C. Winsemius et al., "Global drivers of future river flood risk," Nature Climate Change, vol. 6, pp. 381–385, 2016, doi: 10.1038/nclimate2893.
18. P. J. Ward et al., "Assessing flood risk at the global scale: Model setup, results, and sensitivity," Environmental Research Letters, vol. 8, art. 044019, 2013, doi: 10.1088/1748-9326/8/4/044019.
19. B. Jongman et al., "Declining vulnerability to river floods and the global benefits of adaptation," Proceedings of the National Academy of Sciences, vol. 112, pp. E2271–E2280, 2015, doi: 10.1073/pnas.1414439112.
20. E. E. Koks, B. Jongman, T. G. Husby, and W. J. W. Botzen, "Combining hazard, exposure and social vulnerability to provide lessons for flood risk management," Environmental Science & Policy, vol. 47, pp. 42–52, 2015, doi: 10.1016/j.envsci.2014.10.013.
21. B. Merz, H. Kreibich, R. Schwarze, and A. Thieken, "Assessment of economic flood damage," Natural Hazards and Earth System Sciences, vol. 10, pp. 1697–1724, 2010, doi: 10.5194/nhess-10-1697-2010.
22. G. Aronica, P. D. Bates, and M. S. Horritt, "Assessing the uncertainty in distributed model predictions using observed binary pattern information within GLUE," Hydrological Processes, vol. 16, pp. 2001–2016, 2002, doi: 10.1002/hyp.398.
23. F. Pappenberger, K. Frodsham, K. Beven, R. Romanowicz, and P. Matgen, "Fuzzy set approach to calibrating distributed flood inundation models using remote sensing observations," Hydrology and Earth System Sciences, vol. 11, pp. 739–752, 2007, doi: 10.5194/hess-11-739-2007.
24. J. C. Neal, P. D. Bates, T. J. Fewtrell, N. M. Hunter, M. D. Wilson, and M. S. Horritt, "Distributed whole city water level measurements from the Carlisle 2005 urban flood event and comparison with hydraulic model simulations," Journal of Hydrology, vol. 368, pp. 42–55, 2009, doi: 10.1016/j.jhydrol.2009.01.026.
25. M. S. Horritt and P. D. Bates, "Effects of spatial resolution on a raster based model of flood flow," Journal of Hydrology, vol. 253, pp. 239–249, 2001, doi: 10.1016/S0022-1694(01)00490-5.
26. P. D. Bates and A. P. J. De Roo, "A simple raster-based model for flood inundation simulation," Journal of Hydrology, vol. 236, pp. 54–77, 2000, doi: 10.1016/S0022-1694(00)00278-X.
27. P. D. Bates, "Predicting floodplain inundation: Raster-based modelling versus the finite-element approach," Hydrological Processes, vol. 15, pp. 825–842, 2001, doi: 10.1002/hyp.188.
28. S. Hallegatte, C. Green, R. J. Nicholls, and J. Corfee-Morlot, "Future flood losses in major coastal cities," Nature Climate Change, vol. 3, pp. 802–806, 2013, doi: 10.1038/nclimate1979.

Figures

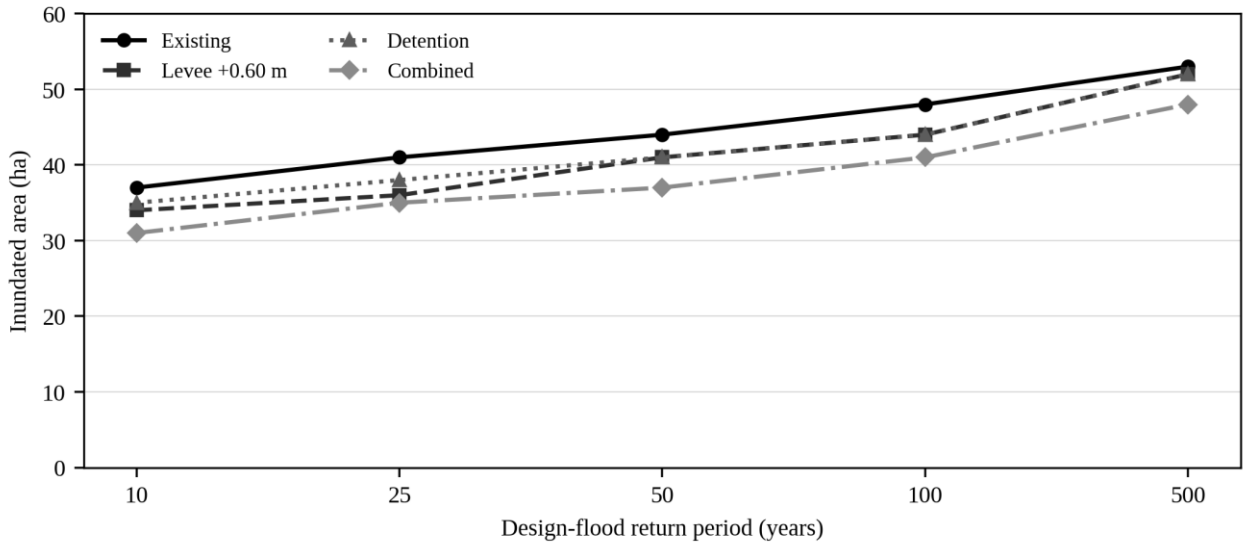

Figure 1. Flooded area under the four alternatives across the five design-flood return periods. Each cell contributes 1 ha to the mapped extent.

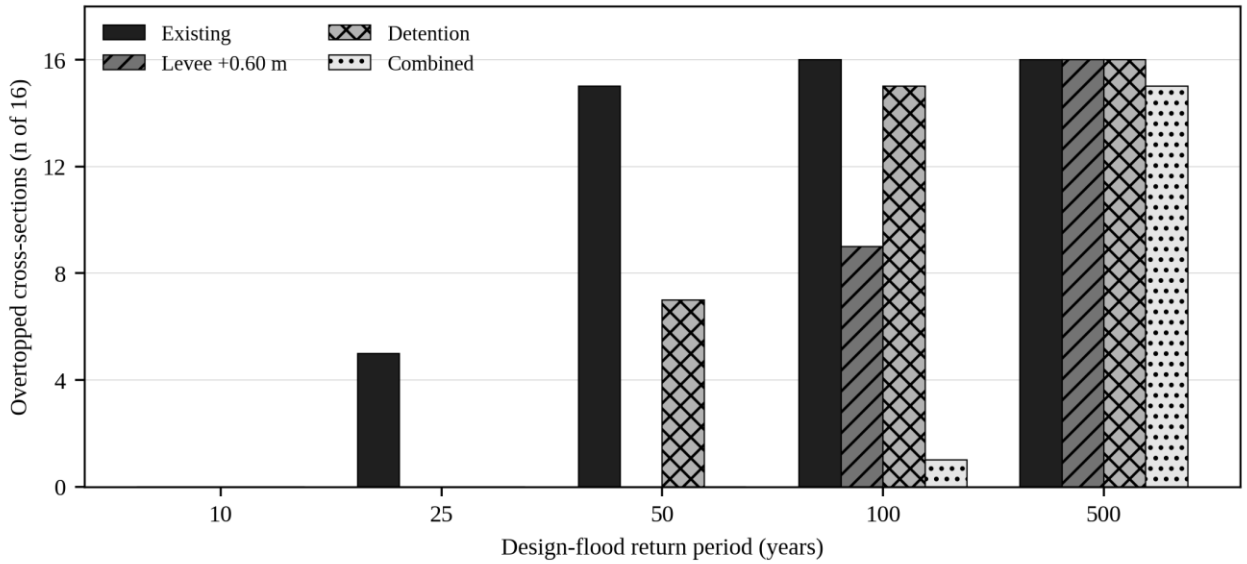

Figure 2. Number of overtopped sections out of 16. The combined design suppresses overtopping through the 50-year case but not under the 500-year flood.

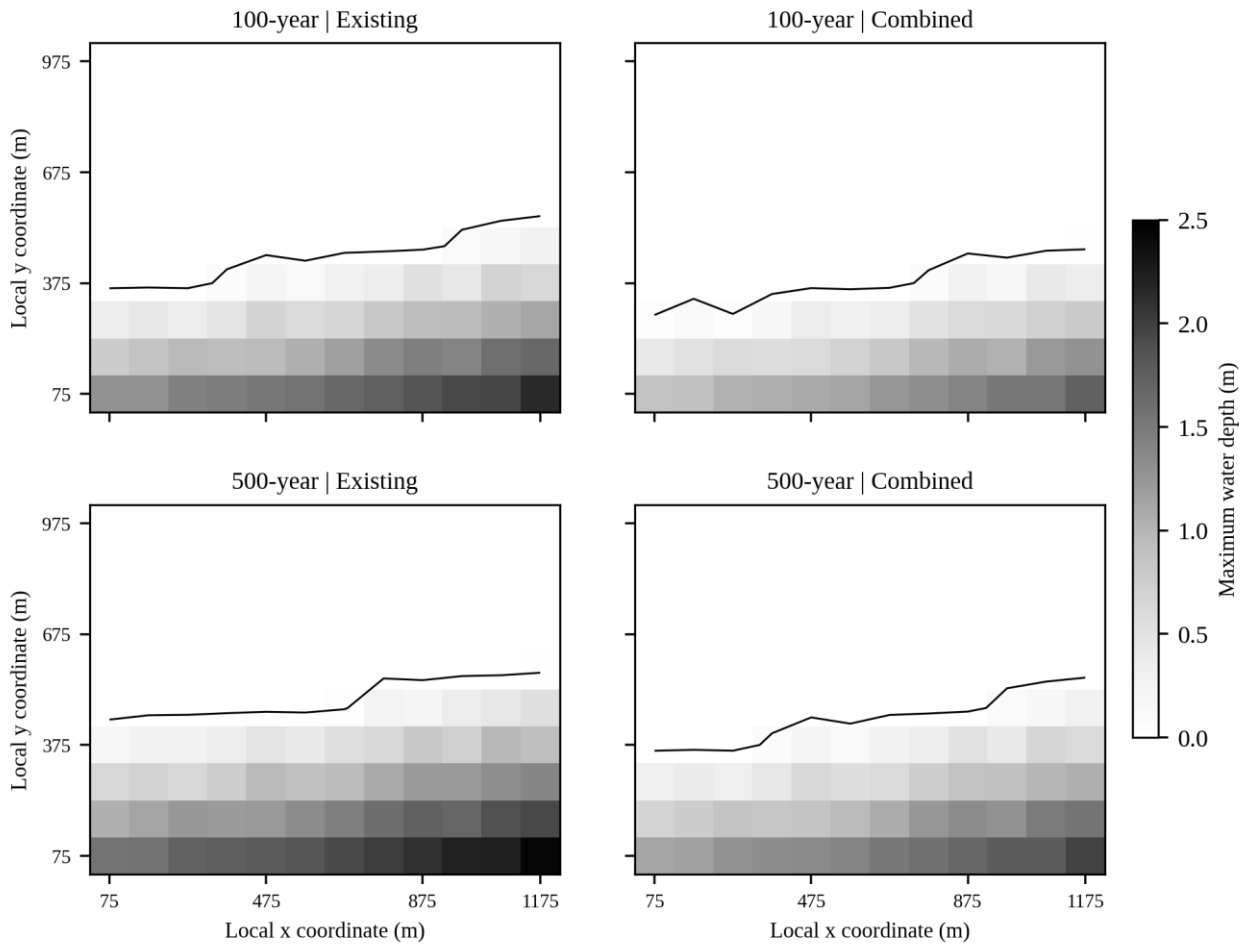

Figure 3. Maximum flood depth at 100 and 500 years under existing and combined protection, shown on the 100-m idealised local grid. Grayscale intensity increases with depth; the black outline marks approximate wet/dry boundaries.

Tables

Table 1. Idealised hydraulic domain and infrastructure configurations

Parameter	Value / specification
Cross-sectional domain	16 sections, 0–6.0 km; widths 24–36 m; Manning n 0.035–0.044
Local floodplain grid	120 × 1-ha cells; 1.20 km²; ground elevation 109.82–112.99 m
Design-event recurrence	10, 25, 50, 100 and 500 years
24-h design precipitation	83, 117, 144, 174 and 258 mm, respectively
Design-event peak component	112, 156, 195, 238 and 345 m³/s, respectively
Existing protection (E)	Reference crest and event peak
Raised levee (L)	Reference event peak; +0.60 m crest
Detention basin (D)	−17% event peak; nominal storage 0.08 × 10⁶ m³
Combined (C)	+0.60 m crest; −17% event peak; 0.08 × 10⁶ m³ storage

Table 2. Hydraulic and exposure outcomes for the 20 design cases

RP (yr)	Alt.	Wet area (ha)	Mean depth (m)	Max depth (m)	Overtop (n)	Built-up wet (n)	Critical wet (n)	H ≥ 1 (n)
10	E	37	0.800	1.780	0	25	15	18
10	L	34	0.643	1.522	0	23	15	14
10	D	35	0.760	1.670	0	24	15	17
10	C	31	0.620	1.420	0	20	15	9
25	E	41	0.853	1.912	5	28	17	21
25	L	36	0.737	1.654	0	25	15	16
25	D	38	0.807	1.776	0	25	15	18
25	C	35	0.656	1.526	0	24	15	14
50	E	44	0.912	2.029	15	29	17	26

RP (yr)	Alt.	Wet area (ha)	Mean depth (m)	Max depth (m)	Overtop (n)	Built-up wet (n)	Critical wet (n)	H ≥ 1 (n)
50	L	41	0.761	1.771	0	28	17	19
50	D	41	0.844	1.871	7	28	17	21
50	C	37	0.713	1.620	0	25	15	15
100	E	48	0.964	2.158	16	32	17	29
100	L	44	0.837	1.900	9	29	17	21
100	D	44	0.892	1.974	15	29	17	26
100	C	41	0.745	1.724	1	28	17	19
500	E	53	1.145	2.434	16	35	19	36
500	L	52	0.969	2.176	16	35	18	33
500	D	52	1.001	2.233	16	35	18	33
500	C	48	0.882	1.982	15	32	17	28

Table 3. Matched-event benefits relative to existing protection

Return period (yr)	Levee area ↓ (%)	Detention area ↓ (%)	Combined area ↓ (%)	Combined mean depth ↓ (%)	High-index cells E → C	Overtopped sections E → C
10	8.1	5.4	16.2	22.5	18 → 9	0 → 0
25	12.2	7.3	14.6	23.1	21 → 14	5 → 0
50	6.8	6.8	15.9	21.8	26 → 15	15 → 0
100	8.3	8.3	14.6	22.7	29 → 19	16 → 1
500	1.9	1.9	9.4	23.0	36 → 28	16 → 15